2. J. J. Thwaites and N. H. Mendelson, *Adv. Microb. Physiol.* **32**, 173 (1991).
3. T. J. Beveridge, in *Metal-Microbe Interactions*, R. K. Poole and G. M. Gadd, Eds. (IRL Press, New York, 1989), pp. 65–83.
4. _____ and R. G. E. Murray, *J. Bacteriol.* **127**, 1502 (1976).
5. R. J. Doyle, in *Metal Ions and Bacteria*, T. J. Beveridge and R. J. Doyle, Eds. (Wiley, New York, 1989), pp. 275–293.
6. R. E. Marquis, K. Mayzel, E. L. Carstensen, *Can. J. Microbiol.* **22**, 975 (1976).
7. M. N. Hughes and R. K. Poole, *Metals and Microorganisms* (Chapman & Hall, New York, 1989), p. 337.
8. H. M. Pooley, *J. Bacteriol.* **125**, 1127 (1976); *ibid.*, p. 1139; J. Chaloupka, L. R. Kreckova, P. Kreckova, *Folia Microbiol. (Prague)* **9**, 9 (1964).
9. J. J. Thwaites and N. H. Mendelson, *Proc. Natl. Acad. Sci. U.S.A.* **82**, 2163 (1985).
10. B. Salhi, thesis, University of Arizona, Tucson (1991).
11. N. H. Mendelson, *Proc. Natl. Acad. Sci. U.S.A.* **73**, 1740 (1976).
12. _____ and J. J. Thwaites, *J. Bacteriol.* **171**, 1055 (1989).
13. S. Mann, in *Biomineralization in Lower Plants and Animals*, B. S. C. Leadbeater and R. Riding, Eds. (Clarendon, Oxford, 1986), pp. 39–45; see also W. E. Krumbein, *ibid.*, pp. 55–72; F. G. Ferris, W. S. Fyte, T. J. Beveridge, *Geology* **16**, 149 (1988).
14. N. H. Mendelson, *Sci. Prog.* **74**, 425 (1990); in *Microbiology—1977*, D. Schlessinger, Ed. (American Society for Microbiology, Washington, DC, 1977), pp. 5–24.
15. T. J. Beveridge and R. G. E. Murray, *J. Bacteriol.* **141**, 876 (1980).
16. H. E. Swaisgood, in *Enzymes and Immobilized Cells in Biotechnology*, A. Laskin, Ed. (Benjamin/Cummings, Menlo Park, CA, 1985), pp. 1–24; G. C. Guilbault, *Analytical Uses of Immobilized Enzymes* (Dekker, New York, 1984).
17. F. G. E. Pautard, in *Biological Calcification*, H. Schraer, Ed. (North-Holland, Amsterdam, 1970), pp. 106–201; R. Y. Morita, *Geomicrobiol. J.* **2**, 63 (1980).
18. R. F. Ziolo *et al.*, *Science* **257**, 219 (1992).
19. A. H. Heuer *et al.*, *ibid.* **255**, 1098 (1992); P. Calvert and S. Mann, *J. Mater. Sci.* **23**, 3801 (1988).
20. P. G. Rouxhet and M. J. Genet, in *Microbial Cell Surface Analysis: Structural and Physico-Chemical Methods*, N. Mozes, P. S. Handley, H. J. Busscher, P. G. Rouxhet, Eds. (VCH, New York, 1991), pp. 173–220.
21. J. H. Miller, *Experiments in Molecular Genetics* (Cold Spring Harbor Laboratory, Cold Spring Harbor, NY, 1972).
22. Supported in part by grants from the National Institute of General Medical Sciences, the University of Arizona and the Arizona Agricultural Experiment Station and a contract from the Air Force Office of Scientific Research. I am indebted to K. W. Nebeshy for XPS measurements, P. D. Calvert for numerous suggestions and guidance, J. J. Thwaites for fiber mechanics measurements, and S. D. Whitworth and H. Fisher for excellent technical assistance.

4 August 1992; accepted 19 October 1992

Electrical Resistivity and Stoichiometry of Ca_xC_{60} and Sr_xC_{60} Films

R. C. Haddon, G. P. Kochanski, A. F. Hebard, A. T. Fiory, R. C. Morris

The temperature- and concentration-dependent resistivities of annealed Ca_xC_{60} and Sr_xC_{60} films were measured near room temperature. Resistivity minima were observed at $x = 2$ and 5. The resistivities of these films were $\rho_{min} \sim 1$ ohm-centimeter for $x = 2$ and $\rho_{min} \sim 10^{-2}$ ohm-centimeter for $x = 5$. This latter value is comparable to the resistivities found in similar experiments on K_3C_{60} films. There is a maximum in the resistivity between $x = 2$ and 3, and another at $x \sim 7$. The conductivity is activated over the whole range of compositions, and the activation energy scales with the logarithm of the resistivity. The results suggest that the conductivity and superconductivity observed in Ca_5C_{60} are associated with the population of bands derived from the t_{1g} level of C_{60}.

Solid C_{60} and C_{70} undergo doping with alkali metals to produce conductors (*1*). For A = K or Rb, the A_3C_{60} phases are superconductors (*2–5*). It has been shown that Ca intercalates into the C_{60} face-centered-cubic lattice to form a solid solution and that a phase transformation occurs near a Ca/C_{60} ratio of 5/1 to produce a simple cubic structure that is a superconductor with a superconducting transition temperature $T_c = 8.4$ K (*6*). Photoemission studies indicate that C_{60} films lead to a metallic state on exposure to Sr vapor (*7*). Insofar as we are aware, no studies have reported on the transport properties of these systems. We present here resistivity measurements of Ca_xC_{60} and Sr_xC_{60} films, as a function of temperature and doping. We find that Ca- and Sr-doped C_{60} films show a resistivity profile that is entirely different from that observed on doping with alkali metals (*1*, *8*). The results suggest that the conductivity and superconductivity observed in Ca_5C_{60} are associated with the population of bands derived from the t_{1g} level of C_{60}. This implies that the most conducting state of the alkaline earth–doped phases arises from C_{60}^{z-} molecules with $6 > z > 12$, perhaps hybridized with Ca states.

We followed the general scheme adopted to study K_xC_{60} films in ultrahigh vacuum (UHV) (*8*), but there were important improvements in the experimental procedure. The UHV chamber used in this work was equipped with a Radak I evaporation source (Luxel Corporation) so that the C_{60} films were grown in situ and were not exposed to O_2 before doping. Results in the literature suggest that exposure of C_{60} films to O_2 leads to changes in the Raman spectrum (*9*), although the exact nature of this effect remains to be clarified. Furthermore, this modification allowed us to establish that the doped films were equilibrated under the conditions of our experiment by subsequent addition of C_{60} to Ca_xC_{60} films. The C_{60} films were grown from material produced in the spark erosion process (*10*) and purified by liquid chromatography (*11*). Films produced in this way consist of random polycrystalline grains of dimension ~60 Å (*12*). The Ca and Sr were deposited by thermal evaporation of the pure metal from a tungsten wire basket (R. D. Mathis Company). The UHV chamber also contains a quartz crystal microbalance so that we could directly monitor the amounts of C_{60} and metal that were deposited. The system was baked before deposition, and the base pressure was below 10^{-8} torr.

In the case of K doping the conductivity responded immediately to the addition of metal to the film (*9*), whereas in the present study a high-temperature anneal was necessary to equilibrate the system and obtain meaningful resistivities. We used thin C_{60} films (100 to 500 Å), in order to reduce the time required for the system to reach equilibrium. The electrical measurements were made with substrates similar to those described previously (*9*), except that we used sapphire as the substrate material and evaporated Al and Ag multilayers for contact pads. The quartz crystal microbalance was calibrated with Rutherford backscattering (RBS) measurements on a C_{60} film grown on clean hydrogen-terminated Si. Ex situ RBS analysis of the Ca and Sr peaks in the doped C_{60} films when combined with the C_{60} determination from the microbalance gave us the film composition. Results obtained at intermediate doping levels confirmed the linearity of the response of the quartz microbalance with deposition, and thus the measurements from the quartz microbalance can be used to obtain the film composition at each resistance determination. We estimate the uncertainty in our derived values of x at ± 0.3, due mainly to nonuniformities in the metal sources and the error in the RBS measurements on thin metal/C_{60} films.

After a number of trial experiments, we used a 1-min anneal at 180°C to equilibrate Ca and Sr in the C_{60} film. With lower temperature anneals (down to 100°C), we obtained essentially the same behavior but the features observed in the resistivity were less distinct. At temperatures above 200°C, there was an increase in the contact resis-

AT&T Bell Laboratories, Murray Hill, NJ 07974.

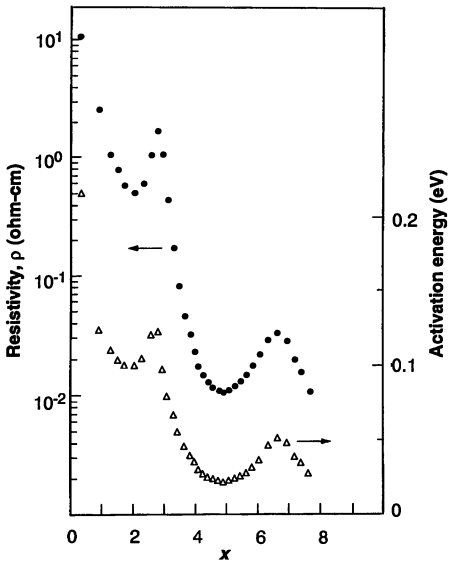

Fig. 1. The resistivity and the activation energy of the conductivity of an annealed Sr_xC_{60} film 190 Å thick at 60°C in UHV as a function of x. The stoichiometry was determined by use of a quartz crystal microbalance and ex situ RBS measurements.

tance of the film, particularly at low doping levels. The resistivity values reported herein were determined at 60°C, and the activation energies were obtained from resistivity data measured in the range 60°C < T < 160°C.

The resistivity and the activation energy are plotted as a function of composition for C_{60} films 190 Å thick in Figs. 1 and 2. The resistivity of the C_{60} film drops on exposure to Sr and reaches a minimum with ρ_{min_1} = 0.5 ohm-cm at a Sr_xC_{60} composition of x = 2.0 (Fig. 1). We estimate that the resistivity maximum occurs at x = 2.9 with $\rho_{max_1} \geq 2.5$ ohm-cm. As x increases, the resistivity drops two more orders of magnitude to another minimum at a Sr_xC_{60} composition of x = 4.9, where $\rho_{min_2} = 1.1 \times 10^{-2}$ ohm-cm. On further doping the resistivity increases until a second maximum is reached at x = 6.6 and $\rho_{max_2} = 3.2 \times 10^{-2}$ ohm-cm.

The results obtained on Ca doping of C_{60} films (Fig. 2) are qualitatively similar to our Sr results, although the features visible in the resistivity data are sharper in the case of Sr than Ca. The first minimum in the Ca_xC_{60} film occurs at x = 2.0 with ρ_{min_1} = 1.0 ohm-cm. The shoulder in the resistivity has x = 2.3 and $\rho_{max_1} \geq 1.1$ ohm-cm. The second minimum occurs at x = 5.0, where $\rho_{min_2} = 5.8 \times 10^{-3}$ ohm-cm, and the second maximum is at x = 7.1 and ρ_{max_2} = 2.2×10^{-2} ohm-cm. The behavior of the Ca_xC_{60} film was very sensitive to annealing in the region x = 2 to 3. Prolonged or high-temperature anneals in this region moved the first maximum toward higher x values, and in some experiments we observed x values of 3 for the maximum. However, irrespective of thermal treatment, the Ca-doped C_{60} films did not show the well-defined minimum and maximum between x = 0 and 3 that is characteristic of Sr doping. In the Sr film shown in Fig. 1 the ratio of ρ_{max_1} to ρ_{min_1} was 5.0, whereas the highest value of this ratio in any Ca-doped film was 1.5.

A further characteristic difference between the two metals is the resistivity value at the minima: the ratio $\rho_{min_1}^{Ca_2C_{60}}/\rho_{min_1}^{Sr_2C_{60}}$ = 2.0, whereas $\rho_{min_2}^{Ca_5C_{60}}/\rho_{min_2}^{Sr_5C_{60}} = 0.5$. Thus, Sr achieves a lower resistivity at the x = 2 composition but Ca has a lower final resistivity at x = 5. Particularly in the case of Ca doping, the resistivity minimum at x = 5 approaches the values reported for K_3C_{60} films: $\rho_{min}^{K_3C_{60}} = 5.5 \times 10^{-3}$ (400 Å film) and 2.2×10^{-3} ohm-cm (>1000 Å film) (8). The value of $\rho_{min_2}^{Ca_5C_{60}} = 5.8 \times 10^{-3}$ ohm-cm may be compared with a value of $\rho_{min}^{K_3C_{60}}$ = 6.3×10^{-3} ohm-cm measured for a film 190 Å thick in the same apparatus.

Beyond x = 5 the resistivity increases until $x \sim 7$. The decrease in resistivity on further doping is presumably the result of conduction by the metal, either as a result of the formation of a Ca or Sr overlayer or perhaps the result of the incorporation of high concentrations of metal atoms into the film itself.

The activation energies for the conduction process were obtained from Arrhenius plots and are included in the lower parts of Figs. 1 and 2. These values parallel the logarithm of the resistivity throughout the doping profile. The activation energy at ρ_{min_1} is higher for Ca_2C_{60} (0.14 eV) than for Sr_2C_{60} (0.10 eV), whereas at ρ_{min_2} it is lower for Ca_5C_{60} (0.018 eV) than for Sr_5C_{60} (0.021 eV), just as is found with the resistivities. In contrast to what was found for K_xC_{60} films, the conduction is activated at all Ca_xC_{60} and Sr_xC_{60} compositions. However, even in the case of the K_3C_{60} granular films, the conductivity is metallic only in the vicinity of room temperature and in the temperature range 200 K > T > 20 K it shows an activated temperature dependence (13). This temperature dependence may reflect the granularity of the pristine C_{60} films (12), which has a marked effect on the transport properties of the resulting K_3C_{60} films (13, 14). Recent resistivity measurements on K_3C_{60} single crystals show a classic metal-like temperature dependence and an extremely sharp superconducting transition (15). Similarly, microwave loss measurements show that T_c is depressed in granular Rb_3C_{60} films (16).

The resistivities may be interpreted in terms of the band structures of these materials (5, 11, 17), and to a first approximation by calculations on the C_{60} molecule

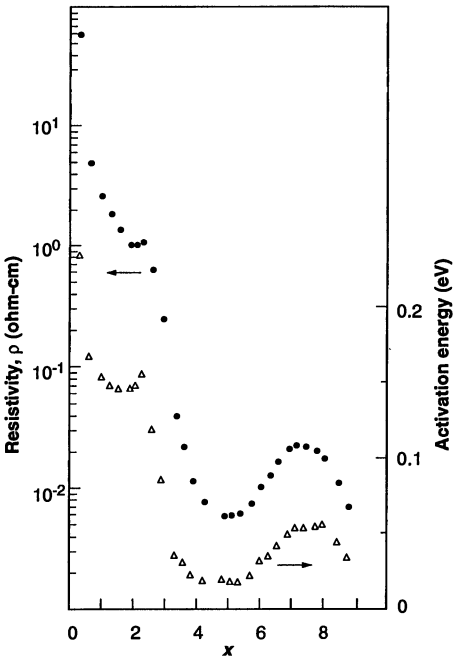

Fig. 2. The resistivity and the activation energy of the conductivity of an annealed Ca_xC_{60} film 190 Å thick at 60°C in UHV as a function of x. The stoichiometry was determined by use of a quartz crystal microbalance and ex situ RBS measurements.

itself (18). The C_{60} molecule has two low-lying, triply degenerate molecular orbitals [t_{1u} lowest unoccupied molecular orbital (LUMO) and t_{1g} LUMO + 1] (5, 7, 18). The first of these, the t_{1u} level, is responsible for the conductivity of the alkali metal–doped A_3C_{60} phases (1). As a result of the high electron affinity of the fullerenes (18, 19), the possibility of populating the next level (t_{1g}) has been discussed (7, 11, 17, 18).

It seems clear that between x = 0 and 3 the electronic structure of the doped C_{60} film is dominated by the population of the t_{1u} level as observed with alkali metal doping. The maximum in the resistivity between x = 2 and 3 suggests that the t_{1u} level becomes filled in this interval. The A_6C_{60} phases are insulators (1, 8), and this behavior is reflected in the Ca_3C_{60} and Sr_3C_{60} films. Nevertheless, particularly in the case of Ca it is apparent that the fully ordered x = 3 phase is difficult to form. Presumably this is a reflection of the poor size match of the third Ca^{2+} to the octahedral site in the C_{60} lattice. The face-centered cubic lattice of C_{60} contains two tetrahedral interstitial sites of radius 1.12 Å and one octahedral interstitial site of radius 2.06 Å per C_{60} molecule (20). The crystal ionic radii of the metals are as follows: Na^+, 0.95 Å; K^+, 1.33 Å; Rb^+, 1.48 Å; Ca^{2+}, 0.99 Å; and Sr^{2+}, 1.13 Å. Thus, if an ionic model is adopted between x = 0 and 3 and the Ca and Sr fully transfer their electrons to C_{60},

then the ionic sizes fall between Na^+ and K^+. Even if the charge transfer is not complete (as suggested by the photoemission results on Sr) (*7*), it is clear that Ca and Sr will be good fits for the tetrahedral sites, and we speculate that Ca_2C_{60} and Sr_2C_{60} are structurally similar to Na_2C_{60} (*21*). In the case of Ca, the weak resistivity maximum probably reflects disorder in the film or a tendency toward disproportionation as a result of the poor size match of the third Ca ion to the interstitial octahedral site. We note that Ca^{2+} is similar in size to Na^+, there is evidence of disorder in the Raman spectrum of Na_3C_{60} films (*22*), and bulk Na_3C_{60} has been shown to undergo a low-temperature disproportionation (*21*).

Beyond $x = 3$ it is therefore apparent that the conductivity is due to carriers in the t_{1g} level, perhaps hybridized with Ca and Sr *s* states as suggested in the photoemission studies (*7*). Thus, the superconductivity observed in bulk Ca_5C_{60} (*6*) apparently originates in bands derived from the t_{1g} level of the C_{60} molecule.

Note added in proof: See the recent photo-emission studies (*23*).

REFERENCES AND NOTES

1. R. C. Haddon *et al.*, *Nature* **350**, 320 (1991).
2. A. F. Hebard *et al.*, *ibid.*, p. 600.
3. M. J. Rosseinsky *et al.*, *Phys. Rev. Lett.* **66**, 2830 (1991).
4. K. Holczer *et al.*, *Science* **252**, 1154 (1991).
5. R. C. Haddon, *Acc. Chem. Res.* **25**, 127 (1992).
6. A. R. Kortan *et al.*, *Nature* **355**, 529 (1992).
7. Y. Chen, F. Stepniak, J. H. Weaver, L. P. F. Chibante, R. E. Smalley, *Phys. Rev. B* **45**, 8845 (1992).
8. G. P. Kochanski, A. F. Hebard, R. C. Haddon, A. T. Fiory, *Science* **255**, 184 (1992).
9. S. J. Duclos, R. C. Haddon, S. H. Glarum, A. F. Hebard, K. B. Lyons, *Solid State Commun.* **80**, 481 (1991).
10. W. Krätschmer *et al.*, *Nature* **347**, 354 (1990).
11. R. C. Haddon *et al.*, in *Fullerenes*, G. S. Hammond and V. J. Kuck, Eds. (ACS Symposium Series 481, American Chemical Society, Washington, DC, 1992), p. 71.
12. A. F. Hebard, R. C. Haddon, R. M. Fleming, A. R. Kortan, *Appl. Phys. Lett.* **59**, 2109 (1991).
13. T. T. M. Palstra, R. C. Haddon, A. F. Hebard, J. Zaanen, *Phys. Rev. Lett.* **68**, 1054 (1992).
14. H. Ogata *et al.*, *Jpn. J. Appl. Phys.* **31**, L166 (1992).
15. X.-D. Xiang *et al.*, *Science* **256**, 1190 (1992).
16. S. H. Glarum, S. J. Duclos, R. C. Haddon, *J. Am. Chem. Soc.* **114**, 1996 (1991).
17. S. Saito and A. Oshiyama, *Solid State Commun.* **83**, 107 (1992).
18. R. C. Haddon, L. E. Brus, K. Raghavachari, *Chem. Phys. Lett.* **125**, 459 (1986).
19. R. F. Curl and R. E. Smalley, *Science* **242**, 1017 (1988).
20. R. M. Fleming *et al.*, *Mater. Res. Soc. Symp. Proc.* **206**, 691 (1991).
21. M. J. Rosseinsky *et al.*, *Nature* **356**, 416 (1992).
22. S. J. Duclos, R. C. Haddon, S. Glarum, A. F. Hebard, K. B. Lyons, *Science* **254**, 1625 (1991).
23. Y. Chen *et al.*, *ibid.* **46**, 7961 (1992); G. K. Wertheim, D. N. E. Buchanan, J. E. Rowe, *Science* **258**, 1638 (1992).

24. We are grateful to P. H. Citrin and C. E. D. Chidsey for the use of UHV equipment, to R. H. Eick for assistance with substrate preparations, and to T. T. M. Palstra for assistance with the conductivity measurements.

30 July 1992; accepted 16 September 1992

Charge Donation by Calcium into the t_{1g} Band of C_{60}

G. K. Wertheim, D. N. E. Buchanan, J. E. Rowe

Photoemission spectra of compounds prepared by the reaction of C_{60} films with calcium show two distinct metallic phases, whereas alkali-doped C_{60} films have only one. In the first phase the bulk t_{1u} band, derived from the lowest unoccupied molecular orbital of C_{60}, is partially occupied. This is followed by an insulating phase that has the composition Ca_3C_{60} in which the t_{1u} band is filled and has properties analogous to those of K_6C_{60}. Continued exposure to calcium produces a second metallic phase in which electrons are donated into the t_{1g} band. The superconductivity of Ca_5C_{60} is associated with the t_{1g} band.

According to a recent report (*1*), Ca_5C_{60} is a superconductor like the A_3C_{60} compounds formed by the alkali metals A = K, Rb, and Cs. In view of the divalent character of Ca, it seems unlikely that the charge donated to the C_{60} is the same in both materials. However, it is not clear from transport measurements alone (*1*) whether the mechanism for conductivity and for superconductivity is the same in Ca-doped fullerides as in alkali compounds.

AT&T Bell Laboratories, Murray Hill, NJ 07974.

Photoemission spectroscopy can answer this question by providing a direct view of the occupied electronic structure. Care must be exercised, however, because this technique probes a surface layer comparable in thickness to the layer spacing of C_{60}. Nevertheless, we can identify the band responsible for the superconductivity, that is, whether it is the t_{1u} band as in the alkali metal compounds or the second empty band derived from the t_{1g} orbitals.

The prospect that the t_{1g} band is occupied at first seemed remote because Chen *et al.* (*2*) report a hybridized band involving only the t_{1u} states of C_{60} and the outer *ns* levels of Mg, Sr, and Ba ($n = 3$, 5, and 6) in other alkaline earth compounds of C_{60}. We report here that Ca_xC_{60} does not conform to this pattern, exhibiting the sequential filling of the t_{1u} and t_{1g} bands with increasing Ca content. We find that the superconductivity is associated with the second unoccupied band of C_{60}, which has t_{1g} symmetry.

Calcium differs from the heavier alkali and alkaline earth ions for which metallic C_{60} intercalation compounds have been reported in having a significantly smaller ionic radius, 0.99 Å, as compared to 1.33,1.47, 1.67, 1.12, and 1.34 Å for K, Rb, Cs, Sr, and Ba, respectively. Other elements with small ionic radii, for example, Na (0.97 Å) and Mg (0.66 Å), are reported to form insulating compounds with C_{60} (*2*, *3*). The tetrahedral sites in C_{60} have a radius of 1.12 Å and can readily accommodate the small Ca^{2+} ion. The octahedral sites are much larger and can accommodate an atom with a radius of 2.06 Å. A small ion like Ca^{2+} will be displaced from the center of the site along one of the eight (111) directions, toward one of the neighboring tetrahedral sites (*1*). It will then contact only three of the six C_{60} molecules that define the octahedral site. Multiple occupancy by up to four ions has been suggested (*1*). However, the incompletely screened Coulomb repulsion between these ions probably makes the site energetically less favorable for additional ions.

The Ca-doped fulleride samples used in this study were prepared as thin films on a W(100) substrate that had been cleaned by sputtering and annealing. Two procedures were used: (i) films of C_{60} 100 to 200 Å thick, deposited from a Knudsen cell onto the room-temperature substrate, were subsequently exposed at room temperature to Ca vapor from another furnace with a BN crucible and (ii) a thick Ca layer was deposited at 78 K followed immediately by a layer of C_{60} 100 Å thick. In the first method data were taken both immediately after exposure and after a brief anneal to 425 K. In the second method measurements were made as this Ca-C_{60} sandwich was annealed at temperatures up to 400 K. We took the photoemission data with 21.2-eV He I resonance radiation, using a 50-mm hemispherical electron-energy analyzer (Vacuum Science Workshop). A nominal instrumental resolution of 100 meV was used throughout. This is sufficiently small compared to the width of the spectral features of both C_{60} and Ca_xC_{60} that the data show no discernible instrumental broadening, except at the Fermi cutoff.

Figure 1 demonstrates the importance of annealing on C_{60} films after exposure to Ca